

# Infrared extrapolations of quadrupole moments and transitions

D. Odell,<sup>1</sup> T. Papenbrock,<sup>1,2</sup> and L. Platter<sup>1,2</sup>

<sup>1</sup>*Department of Physics and Astronomy, University of Tennessee, Knoxville, Tennessee 37996, USA*

<sup>2</sup>*Physics Division, Oak Ridge National Laboratory, Oak Ridge, Tennessee 37831, USA*

We study the convergence of bound-state quadrupole moments in finite harmonic oscillator spaces. We derive an expression for the infrared extrapolation for the quadrupole moment of a nucleus and benchmark our results using different model interactions for the deuteron. We find good agreement between the analytically derived and numerically obtained convergence behavior. We also derive an extrapolation formula for electric quadrupole transitions and find good agreement with the numerical calculation of a simple system.

## I. INTRODUCTION

The numerical calculation of observables of strongly interacting systems requires frequently the use of truncated Hilbert spaces. For example, lattice quantum chromodynamics (QCD) simulations are usually carried out in a finite volume with periodic boundary conditions. Nuclear structure calculations employ frequently the harmonic oscillator (HO) basis as it preserves rotational symmetry and facilitates a straightforward way of separating out the center-of-mass motion, see, e.g., Refs. [1, 2]. Such calculations require clearly a quantitative and qualitative understanding of the corrections due to the involved Hilbert space truncation, and in lattice QCD the general form of these corrections were derived for a number of observables by Lüscher approximately 30 years ago [3]. For nuclear structure calculations in the HO basis it was only recently understood that the truncated HO can be thought of as imposing long-range, hard-wall boundary conditions with an additional short distance regulator [4]. Specifically, it was found that a HO basis consisting of  $N$  oscillator shells with oscillator length  $b$  has an ultraviolet (UV) cutoff [5]

$$\Lambda \approx \sqrt{2N}/b, \quad (1)$$

while the infrared (IR) cutoff and therefore the spatial extent of the basis is approximately [6, 7]

$$L \approx \sqrt{2Nb}. \quad (2)$$

Relations (1) and (2) are leading-order approximations and valid for  $N \gg 1$ . A more precise expression for an HO in three dimensions was derived in Ref. [8]

$$L = \sqrt{2(N_{\max} + 3/2 + 2)b}. \quad (3)$$

Here,  $b = \sqrt{\hbar/(\mu\Omega)}$ ,  $\mu$ , and  $\Omega$  denote the oscillator length, the reduced mass and the oscillator frequency, respectively. We note that Eq. (3) is specific to a two-body system in relative coordinates (or a single particle in three dimensions). Precise values for the IR length scale  $L$  were also derived for many-body product spaces [9], and no-core shell model spaces [10].

Coon *et al.* [11] found that ground-state energies converge exponentially with the IR length  $L$ . This convergence can be understood as follows [4]. The finite extent  $L$  of the oscillator basis in position space imposes a Dirichlet boundary condition of the bound-state wave function at  $r = L$ . The exponential convergence in  $L$  is thus directly related to the exponential fall-off of bound-state wave functions in position space. These insights led to theoretically founded IR extrapolation formulas [4, 12] for bound-state energies

$$E_L = E_\infty + a_0 e^{-2k_\infty L}, \quad (4)$$

and radii

$$\langle \hat{r}^2 \rangle_L \approx \langle \hat{r}^2 \rangle_\infty - [c_0(k_\infty L)^3 + c_1 k_\infty L] e^{-2k_\infty L}. \quad (5)$$

Here  $a_0$ ,  $k_\infty$ ,  $E_\infty$ , and  $c_0$ ,  $c_1$ , and  $\langle \hat{r}^2 \rangle_\infty$  are determined by fitting to numerical data in many-body systems.

In both cases (as well as for the quadrupole moment extrapolation derived below) the  $e^{-2k_\infty L}$  term comes from the universal long-range behavior of the radial wave function,  $\mathcal{R}_l(r)$ . The spherical Hankel functions,  $h_l(\pm ikr)$ , are the negative-energy solutions in the free region, and imposing a Dirichlet boundary condition at  $r = L$  gives a solution of the form

$$\mathcal{R}_l(r) = h_l(ikr) + Ch_l(-ikr), \quad (6)$$

where  $C = e^{-2kL}$  in leading order for  $kL \gg 1$ .

In this work, we derive an IR extrapolation formula for the quadrupole moment

$$\langle \mathbf{r}' | \hat{Q} | \mathbf{r} \rangle = e \sqrt{\frac{\pi}{5}} r^2 Y_{20}(\theta, \phi) \delta^{(3)}(\mathbf{r} - \mathbf{r}') , \quad (7)$$

and take the deuteron as an example. For the deuteron,  $r$  is the relative coordinate. While computing the deuteron's quadrupole moment poses no challenge in HO model spaces, it is already challenging to compute quadrupole moments in  $p$ -shell nuclei that are converged with respect to the size of the HO model space, see Refs. [13–15] for examples. This motivates us to study the IR convergence for bound-state expectation values of the quadrupole moment and for  $E2$  transition matrix elements between bound states.

This paper is organized as follows. We derive an extrapolation formula for the deuteron's quadrupole moment and study our result for a toy model and a realistic nucleon-nucleon interaction. We then generalize the extrapolation formula to the general case where the bound-state wave functions mixes partial waves with orbital angular momenta  $l$  and  $l + 2$ , respectively, or where the bound-state has a finite  $l > 0$ . Finally, we also derive an IR extrapolation formula for  $E2$  transition matrix elements between bound states. We conclude with a summary.

## II. DERIVATION

### A. Deuteron

The deuteron is a spin-1 state

$$|\Psi\rangle = |\Psi_0\rangle + \eta |\Psi_2\rangle , \quad (8)$$

superposed of an  $S$ -state  $\Psi_0$  and a  $D$ -state  $\Psi_2$ . The  $d$ -state amplitude is denoted by  $\eta$ . Without loss of generality we focus on the state with maximum  $J_z = 1$  spin projection. The wave function for a state with orbital angular momentum  $l$  is

$$\Psi_l(r, \theta, \phi) = \mathcal{R}_l(r) \sum_{m, m_s} C_{l, m; 1, m_s}^{1, 1} Y_{l, m}(\theta, \phi) \chi_{s, m_s} . \quad (9)$$

Here  $\mathcal{R}_l(r)$  denotes the solution to the radial Schrödinger equation. The orbital angular momentum, represented by the spherical harmonics  $Y_{lm}(\theta, \phi)$ , and spin, represented by the spinor  $\chi_{s, m_s}$ , are coupled to a total angular momentum  $J = 1$  by means of the Clebsch-Gordan coefficient  $C_{l, m; 1, m_s}^{1, 1}$  [16].

For the computation of the IR correction of the quadrupole moment we follow closely the corresponding derivation made in Ref. [12] for the radius squared. In a finite oscillator basis with IR length scale  $L$ , the expectation value of the quadrupole moment (7) will differ from the infinite-space result, and

$$Q_L = Q_\infty + \Delta Q_L . \quad (10)$$

Here

$$\Delta Q_L = \frac{\langle \Psi_L | \hat{Q} | \Psi_L \rangle}{\langle \Psi_L | \Psi_L \rangle} - \frac{\langle \Psi_\infty | \hat{Q} | \Psi_\infty \rangle}{\langle \Psi_\infty | \Psi_\infty \rangle} , \quad (11)$$

defines the expressions for  $Q_L$  and  $Q_\infty$  such that any  $L$ -independent terms will cancel in Eq. (11). The wave functions  $\Psi_L$  and  $\Psi_\infty$  are the deuteron wave functions in the finite and infinite oscillator spaces, respectively.

Using Eqs. (8) and (9), four terms enter the expectation value in the first term of Eq. (11), and

$$\begin{aligned} \langle \Psi_L | \hat{Q} | \Psi_L \rangle = e \sqrt{\frac{\pi}{5}} \int_0^L \int_0^\pi \int_0^{2\pi} dr r^2 d\theta \sin \theta d\phi \left[ \mathcal{R}_{L,0} Y_{00}^* \chi_1^\dagger + \eta \mathcal{R}_{L,2} \sum_{m, m_s} C_{2, m; 1, m_s}^{1, 1} Y_{2m}^* \chi_{m_s}^\dagger \right] \\ \times r^2 Y_{20} \left[ \mathcal{R}_{L,0} Y_{00} \chi_1 + \eta \mathcal{R}_{L,2} \sum_{m, m_s} C_{2, m; 1, m_s}^{1, 1} Y_{2m} \chi_{m_s} \right] . \end{aligned} \quad (12)$$

The expectation value in the second term on the right-hand side of Eq. (11) is found by replacing  $L$  by  $\infty$ . The  $S$ - $S$  term is zero, so we have only to consider the remaining  $S$ - $D$  mixing terms and the  $D$ - $D$  term. Our interest is in the

$L$ -dependence of the quadrupole moment which is contained entirely in the radial integrations carried out in the first term on the right-hand side of Eq. (11)

$$\int_0^L dr r^4 \mathcal{R}_{L,0}(r) \mathcal{R}_{L,2}(r) , \quad (13)$$

and

$$\int_0^L dr r^4 \mathcal{R}_{L,2}(r) \mathcal{R}_{L,2}(r) . \quad (14)$$

We assume that the nuclear potential vanishes beyond  $r = R$  and split the radial integration into two parts. In general,

$$\int_0^L dr r^4 \mathcal{R}_{L,l_1}(r) \mathcal{R}_{L,l_2}(r) = \int_0^R dr r^4 \mathcal{R}_{L,l_1}(r) \mathcal{R}_{L,l_2}(r) + \int_R^L dr r^4 \mathcal{R}_{L,l_1}(r) \mathcal{R}_{L,l_2}(r) . \quad (15)$$

The interior region, between 0 and  $R$ , depends primarily on the details of the interaction. Around  $E_\infty$  one assumes that the radial wave function  $\mathcal{R}_{L,l}$  in  $L$ -space can be expanded in terms of the radial wave function in infinite space  $\mathcal{R}_{\infty,l}$  and a correction term, e.g. by using the linear energy method [17]. The resulting  $L$ -dependence from the integration over the interior region scales as  $\mathcal{O}(L^0)e^{-2kL}$  [12] and therefore does not contribute to the dominant correction terms [the polynomial in  $kL$  at  $\mathcal{O}(e^{-2kL})$ ]. We therefore concentrate on the second region between  $R$  and  $L$ , and consider the integrals

$$\int_R^L dr r^4 \mathcal{R}_{L,0}(r) \mathcal{R}_{L,2}(r) , \quad (16)$$

and

$$\int_R^L dr r^4 \mathcal{R}_{L,2}(r) \mathcal{R}_{L,2}(r) , \quad (17)$$

in the region free from the potential. Here, the radial wave functions are

$$\begin{aligned} \mathcal{R}_{L,0}(r) &= h_0(ik_L r) + C_0 h_0(-ik_L r) \\ &= -\frac{e^{-k_L r}}{k_L r} + C_0 \frac{e^{k_L r}}{k_L r} , \end{aligned} \quad (18)$$

with

$$C_0 = -\frac{h_0(ik_L L)}{h_0(-ik_L L)} = e^{-2k_L L} , \quad (19)$$

and

$$\begin{aligned} \mathcal{R}_{L,2}(r) &= h_2(ik_L r) + C_2 h_2(-ik_L r) \\ &= \frac{e^{-k_L r}}{(k_L r)^3} [(k_L r)^2 + 3k_L r + 3] - C_2 \frac{e^{k_L r}}{(k_L r)^3} [(k_L r)^2 - 3k_L r + 3] , \end{aligned} \quad (20)$$

with

$$C_2 = -\frac{h_2(ik_L L)}{h_2(-ik_L L)} = e^{-2k_L L} \frac{(k_L L)^2 + 3k_L L + 3}{(k_L L)^2 - 3k_L L + 3} . \quad (21)$$

The coefficients  $C_0$  and  $C_2$  are chosen such that the wave function vanishes at  $r = L$ .

Finally, we sum the  $S$ - $S$  and  $S$ - $D$  terms and expand in powers of  $e^{-2kL}$ . We consider the leading order (LO) term,  $Q_\infty$ , and the next-to-leading order (NLO) term which contains a polynomial in  $kL$  times  $e^{-2kL}$ . We restrict our analysis to the highest powers of  $kL$  and arrive at

$$Q_L = Q_\infty - a(k_\infty L)^3 \left(1 + \frac{d}{k_\infty L}\right) e^{-2k_\infty L} , \quad (22)$$

with corrections of order  $\mathcal{O}(k_\infty L e^{-2k_\infty L})$ . Here  $Q_\infty$ ,  $a$ ,  $d$ , and  $k_\infty$  can be treated as fit parameters. Note that to LO,  $k_L \approx k_\infty$ , where (in the two-nucleon system)

$$k_L = k_\infty - \gamma_\infty^2 e^{-2k_\infty L} + \mathcal{O}(e^{-4k_\infty L}) , \quad (23)$$

and  $\gamma_\infty$  is the asymptotic normalization coefficient [12]. The LO term is all we need to determine the polynomial at  $\mathcal{O}(e^{-2k_\infty L})$  for  $Q_L$ .

### B. Generalized angular momentum states

We can apply this reasoning to a system with an arbitrary mixture of  $l$  states, i.e.

$$|\Psi\rangle = |\Psi_{l_1}\rangle + \eta |\Psi_{l_2}\rangle . \quad (24)$$

For simplicity we limit ourselves to LO and consider only the asymptotic form

$$h_l(\rho) \rightarrow \frac{i}{\rho} e^{-i(\rho - \frac{l\pi}{2})} , \quad (25)$$

of the spherical Hankel functions at large  $\rho$ . As before, if we consider  $\pm i\rho$  (where  $\rho = kr$ ) solutions and enforce the boundary condition at  $r = L$ , we have for the radial behavior

$$\mathcal{R}_{L,l}(k_L r) = -\frac{1}{k_L r} e^{i\pi l/2} (e^{-k_L r} - e^{-2k_L L} e^{k_L r}) . \quad (26)$$

Computing the quadrupole moment expectation value again gives four terms. But when we consider the radial integrations

$$\int_R^L dr r^4 \mathcal{R}_{L,l_1}^*(r) \mathcal{R}_{L,l_1}(r) , \quad (27)$$

$$\int_R^L dr r^4 \mathcal{R}_{L,l_1(l_2)}^*(r) \mathcal{R}_{L,l_2(l_1)}(r) , \quad (28)$$

$$\int_R^L dr r^4 \mathcal{R}_{L,l_2}^*(r) \mathcal{R}_{L,l_2}(r) , \quad (29)$$

the  $l$  dependence is either cancelled [as in Eq. (27) and Eq. (29)] or attributed to a phase [as in Eq. (28)], and they sum to give similar results. Limiting ourselves to LO, we find

$$Q_L = Q_\infty - a(k_\infty L)^3 e^{-2k_\infty L} . \quad (30)$$

We see that the general case agrees in LO with the particular case (22) for the deuteron. Furthermore, Eq. (30) also applies to quadrupole expectation values of bound-states with finite orbital angular momentum  $l > 0$  but no mixing of partial waves. This makes Eq. (30) the main result of this Subsection. Higher-order corrections depend on orbital angular momenta involved in the particular case under consideration.

### C. Electric quadrupole transitions

The quadrupole moment operator also describes electric quadrupole ( $E2$ ) transitions. If we consider a simple model where the initial state is a pure  $D$ -wave state and the final state is a pure  $S$ -wave state, the amplitude for such a transition is

$$\mathcal{A} = \langle \Psi_0 | \hat{Q} | \Psi_2 \rangle . \quad (31)$$

As before, computing such an amplitude in a truncated basis effectively imposes a Dirichlet boundary condition on the wave functions. Likewise, we can describe the amplitude in the truncated basis ( $\mathcal{A}_L$ ) as the amplitude in the infinite basis ( $\mathcal{A}_\infty$ ) plus a correction term.

$$\mathcal{A}_L = \mathcal{A}_\infty + \Delta\mathcal{A}_L , \quad (32)$$

where

$$\mathcal{A}_L \equiv \langle \Psi_{L,0} | \hat{Q} | \Psi_{L,2} \rangle , \quad (33)$$

$$\mathcal{A}_\infty \equiv \langle \Psi_{\infty,0} | \hat{Q} | \Psi_{\infty,2} \rangle , \quad (34)$$

and we seek to compute  $\Delta\mathcal{A}_L$ . We note that the bound-state momentum  $k_l$  depends on the state  $\Psi_l$ . With  $\Psi_l$  from Eq. (9), and the radial wave functions from Eqs. (18) and (20) for  $\Psi_{L,0}$  and  $\Psi_{L,2}$ , respectively, we can easily derive an expression for  $\mathcal{A}_L$ . Essentially, we need to evaluate Eq. (16) for states with different angular momenta (or different  $k_l$  values). While the procedure is similar to the calculation of quadrupole moments, the result is somewhat more complex. We obtain (written explicitly as a function of  $L$ )

$$\mathcal{A}_L = \mathcal{A}_\infty + a_0 \left[ 1 + \frac{a_1}{k_2 L} + \mathcal{O} \left( \frac{1}{(k_2 L)^2} \right) \right] e^{-2k_2 L} , \quad (35)$$

where terms of  $\mathcal{O}[(k_0 + k_2)L e^{-(k_0 + k_2)L}]$  and higher have been dropped. Here,  $k_0$  and  $k_2$  represent the  $S$ - and  $D$ -wave binding momenta, respectively (as  $k_\infty$  previously represented the separation energy in the case of the deuteron), and the constants  $a_0$  and  $a_1$  are fit parameters.

In general,  $E2$  transitions might occur between any states of identical parities whose angular momenta differ by at most two units. Employing the asymptotic form (25), we find that the transition between bound states with angular momenta  $l_1$  and  $l_2$  and bound-state momenta  $k_1$  and  $k_2$ , respectively extrapolates as

$$\mathcal{A}_L = \mathcal{A}_\infty + a_0 e^{-2k_{<} L} . \quad (36)$$

Here,  $k_{<} \equiv \min(k_1, k_2)$ . The general LO formula (36) is the main result of this Subsection. One might be surprised that the LO formula (36) for  $E2$  transitions differs from the LO formula (30) for expectation values by the absence of the factor proportional to  $L^3$ . Inspection shows that the limit  $k_1 \rightarrow k_2$  is interesting because terms with prefactors involving  $(k_1 - k_2)^{-3}$  become proportional to  $L^3$  in this limit.

## III. RESULTS

### A. Quadrupole moment in a square-well model

As a first test of our analysis, we use a toy model for the deuteron consisting of a square-well potential for the central and a tensor interaction,  $V = V_{\text{sq}} + V_{\text{T}}$ , with

$$V_{\text{sq}} = -V_0 \Theta(R - r) , \quad (37)$$

and

$$V_{\text{T}} = \alpha V_{\text{sq}} S_{12} . \quad (38)$$

Here

$$\begin{aligned} S_{12} &= \vec{Y}_2 \cdot \vec{X}_2 \\ &= \sum_{\mu} (-1)^{\mu} Y_{2,\mu} X_{2,-\mu} , \end{aligned} \quad (39)$$

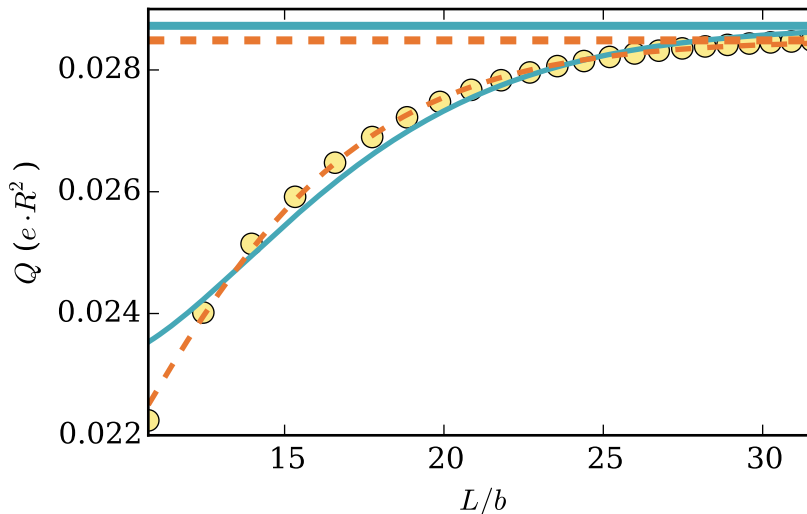


FIG. 1. (color online) Convergence of the quadrupole moment for the deuteron modeled by a simple square well potential as a function of the infrared length  $L$  (given in units of the oscillator length  $b$ ). The yellow circles are the data from the computation. The thin, blue, solid line is the fit to Eq. (30). The thin, orange dashes are the fit to Eq. (22). The thick, blue, solid line is  $Q_\infty$  from the fit to Eq. (30). The thick, orange dashes are  $Q_\infty$  from the fit to Eq. (22).

consists of the rank-two tensor  $\vec{Y}_2$  with components  $Y_{2\mu}$ , and

$$\begin{aligned} \vec{X}_{2\mu} &\equiv (\vec{\sigma} \times \vec{\sigma})_\mu^{(2)} \\ &= \sum_{m_s, m'_s} C_{1, m_s; 1, m'_s}^{2, \mu} \sigma_{m_s} \sigma_{m'_s}, \end{aligned} \quad (40)$$

is the rank-two spherical tensor obtained from coupling two spins.

We use units such that  $\hbar = 1$ ,  $\mu = 1$ , and  $R = 1$ . For the model parameters we set  $V_0 = 1.83$  (in units of  $(\mu R^2)^{-1}$ ), and  $\alpha = 0.5$ . This yields a  $d$ -state probability of about 4.1%, a ground-state energy of about  $E \approx -0.41$  (in units of  $(\mu R^2)^{-1}$ ), and a squared radius of about  $\langle \hat{r}^2 \rangle \approx 0.36$  (in units of  $R^2$ ).

We perform the diagonalization in the HO basis and compute the quadrupole moment for an increasing number  $N$  of oscillator shells. We choose  $\Omega = 28$  (in units of  $(\mu R^2)^{-1}$ ) yielding an oscillator length  $b = 1/\sqrt{28}$  (in units of  $R$ ) and  $L = \sqrt{2(N + 3/2 + 2)}b$ . The results are shown in Fig. 1. The oscillator frequency is chosen such that  $b \ll R$ ; the smallest length scale from the basis scales as  $b/\sqrt{N}$  and is thus adequate for a numerical diagonalization.

For the quadrupole extrapolation, we first extrapolate the energy (4) and obtain the bound-state momentum  $k_\infty$  from  $E_\infty \equiv -(\hbar k_\infty)^2/(2\mu)$ . The expression in Eq. (22) for the quadrupole extrapolation can be fit in several ways. We will first consider only the dominant term,  $(k_\infty L)^3$ , and fit to Eq. (30), treating  $a$  and  $Q_\infty$  as fit parameters. The extrapolated  $Q_\infty$  value is within 1% of the maximum  $Q_\infty$  value ( $N_{\max} = 500$ ) when fitting to values of  $L$  as low as  $L = 2.0$ . Even fitting to the data within a short range ( $3.0 \leq L \leq 3.5$ ) provides an asymptotic value within a percent of the value calculated by fitting to the largest  $L$  value. We also fit to Eq. (22), as shown in Fig. 1. Including the extra fit parameter,  $d$ , does not impact the extrapolated value significantly, though it can influence the ranges of data over which we can accurately fit.

## B. Realistic deuteron quadrupole moment

For an accurate model of the deuteron, we used the interaction from chiral effective field theory (EFT) as described in Ref. [18]. For the quadrupole fits, we take the bound-state momentum  $k_\infty$  from the known binding energy of the deuteron for this interaction. Fits of the quadrupole moment to Eqs. (22) and (30) yield virtually identical results and are shown in Fig. 2 and Table I.

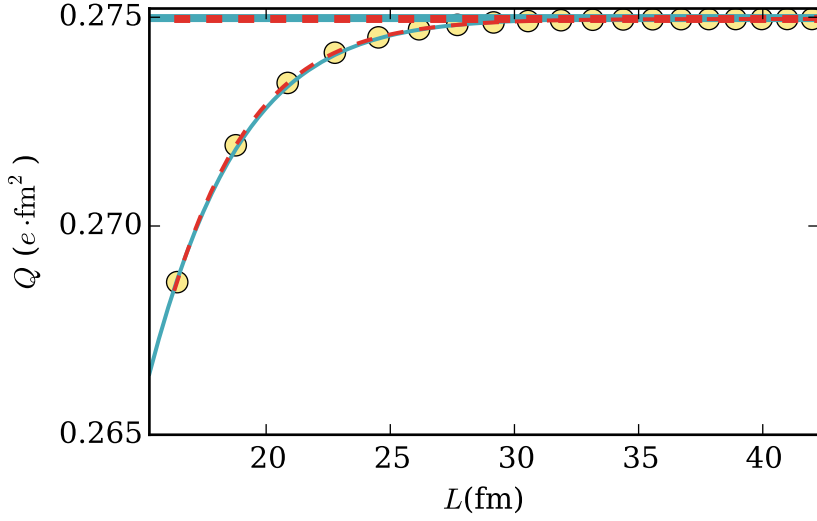


FIG. 2. (color online) Extrapolation of the deuteron quadrupole moment computed from a chiral potential. The yellow circles are the data from the calculation. The thin, blue, solid line is the fit to Eq. (30). The thick, blue, solid line is  $Q_\infty$  from the fit to Eq. (30). The thin, red dashes are the fit to Eq. (22), and the thick, red dashes are  $Q_\infty$  from the fit to Eq. (22).

$L_{\min}$	$L_{\max}$	$Q_\infty^{(30)}$	$Q_\infty^{(22)}$
20	42.40	0.2750	0.2750
15	42.40	0.2750	0.2750
10	42.40	0.2750	0.2750
10	20	0.2768	0.2740
20	30	0.2750	0.2750

TABLE I.  $L_{\min}$  and  $L_{\max}$  (in fm) are the range over which the data is fit.  $Q_\infty^{(30)}$  and  $Q_\infty^{(22)}$  are the extrapolated quadrupole moments (in  $e \cdot \text{fm}^2$ ) when fitting the Eq. (30) and Eq. (22) respectively.

To illustrate the robustness of the extrapolations, we employ different bound-state momenta, namely  $k_\infty$  from the separation energy,  $k_E$  from a fit of the extrapolation (4) to the ground-state energy, and  $k_Q$  from a fit of the quadrupole extrapolation formulas (22) and (30), respectively, in the extrapolation formulas. While the values for the bound-state momenta can differ by as much as 20%, the extrapolated quadrupole moments  $Q_\infty$  differ by only about 1%.

Let us compare the differences between fitting to Eq. (22) and Eq. (30). Figure 3 shows that fitting to the more precise Eq. (22) improves the convergence consistently. We note, however, that the difference in the extrapolated values is almost negligible.

One might also try to extract higher-order corrections to the quadrupole moment that are smaller than  $\mathcal{O}((k_\infty L)^2 e^{-2k_\infty L})$ . These are terms proportional to  $(k_\infty L)^m e^{-2k_\infty L}$  with  $m \leq 1$ , and terms proportional to  $e^{-4k_\infty L}$ . We define (with  $Q(L) \equiv Q_L$ )

$$\delta Q_m = \frac{Q_{\text{calculated}} - Q_{m+1}(L)}{c_m (k_\infty L)^m}, \quad (41)$$

where

$$Q_m(L) = \sum_{n=m}^3 c_n (k_\infty L)^n e^{-2k_\infty L}, \quad (42)$$

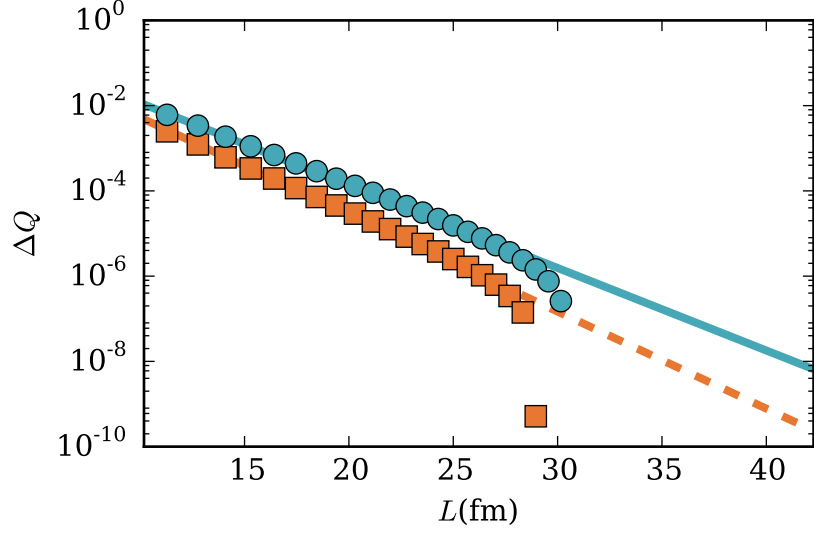


FIG. 3. Difference between the  $L$ -dependent quadrupole moment and its asymptotic value from an extrapolation based on Eq. (30) (blue circles are data and the solid blue line is the fit) and from an extrapolation based on the more precise Eq. (22) (orange squares are data and the dashed orange line is the fit).

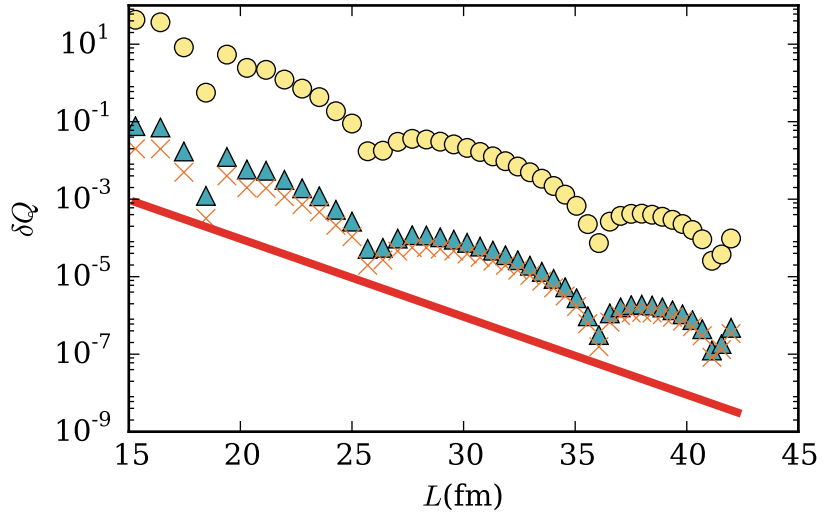


FIG. 4. (color online) The yellow circles represent  $\delta Q_1$  as defined by Eq. (41). The blue triangles represent  $\delta Q_0$ . The orange crosses represent  $\delta Q_{-1}$ . The red line is proportional to  $e^{-2k_\infty L}$ .

is the data reproduced with the fit parameters (represented by  $c_n$  and  $c_m$ ). If we plot  $\delta Q$  alongside what we expect analytically, we ought to be able to establish trends for the higher order corrections. The results are shown in Fig. 4. The overall slopes of the corrections match well with the predicted slope, and as each lower order of  $(k_\infty L)$  is included, the data approaches the  $e^{-2k_\infty L}$  line as expected, supporting the validity of our analysis.

### C. Electric quadrupole transitions

To test our result (35) for  $E2$  transitions, we employ a Hamiltonian with a Gaussian well potential

$$V(r) = -V_0 e^{-\left(\frac{r}{R}\right)^2}, \quad (43)$$



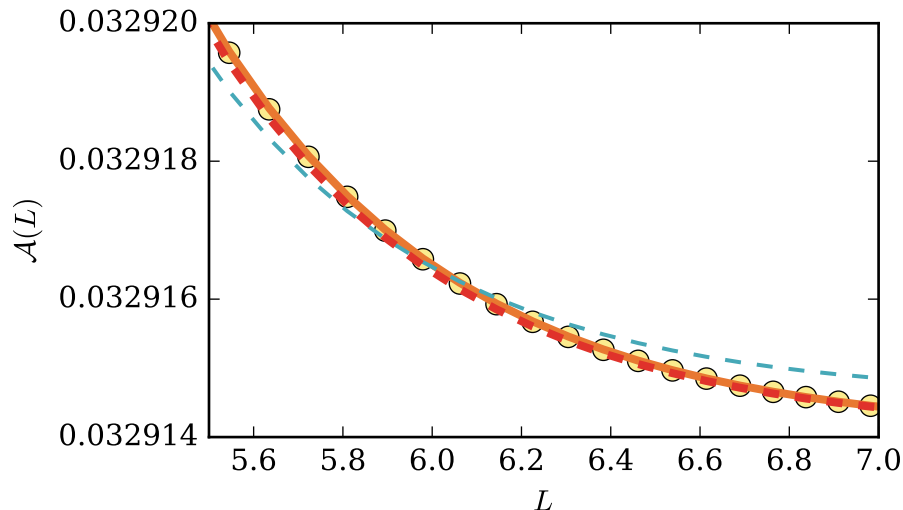


FIG. 5. (color online) Convergence of the  $E2$  transition amplitude in  $e \cdot fm^2$  as a function of  $L$  in units of the  $R$  (the range of the interaction) for a simple Gaussian well model. The yellow dots are the results of the numerical calculation. The thin, light blue dashes are the fit to the leading order result in Eq. (35). The thick, red dashes correspond to a fit including the  $(1/k_2L)^2$  term in Eq. (35). And the solid orange line includes the  $(1/k_2L)^3$  term in the fit.

that is deep enough to contain a bound  $D$ -wave state as well as the ground  $S$ -wave state. As parameters we choose  $R = 1$  and  $V_0 = 15$  (in units of  $(\mu R^2)^{-1}$ ). Recall that the bound-state momenta of the  $S$ - and  $D$ -states are  $k_0$  and  $k_2$ , respectively. Because  $k_2 < k_0$ , the dominant correction contains the exponential  $e^{-2k_2L}$ . Below, we consider three different orders of the polynomial in  $k_2L$  preceding the exponential  $e^{-2k_2L}$  that governs the correction term. From Fig. 5 we can see that the data is more accurately described as increasing powers of  $1/(k_2L)$  are considered. However, over large ranges of  $k_2L$ , which we are able to take advantage of in the simple model presented here, the leading order result can be sufficient to obtain accurate asymptotic values. Figure 5 highlights a small region where the differences in the fitting can be seen. Lower and higher values of  $L$  do not show significant differences.

The log-scale plot, shown in Fig. 6, reveals the differences between the fits and, more importantly, the improvement as higher orders of  $(1/k_2L)$  are included. Here, we plot the residual transition amplitude, *i.e.* the difference between the values calculated in the truncated basis ( $\mathcal{A}_{\text{calculated}}$ ) and the values reproduced by the fit parameters ( $\mathcal{A}_\infty$  and  $c_n$ ). We define

$$\delta\mathcal{A}_m = \frac{\mathcal{A}_{\text{calculated}} - \mathcal{A}_\infty}{\sum_{n=m}^0 c_n (k_2L)^n}, \quad (44)$$

where  $m < 0$ , and we plot the result in Fig. 6 as a measure of how well the fit describes the data for different  $m$  values. Little improvement comes from the  $m = -2$  term due to its small coefficient. Most importantly, we can see that the deviation of the data from the expected behavior happens at larger and larger  $L$  values as more terms in the polynomial factor are included.

#### IV. SUMMARY

We derived IR extrapolation formulas for bound-state quadrupole moments and for quadrupole transitions between bound states in finite oscillator spaces. For two-body systems, the extrapolations are of the form  $(kL)^n e^{-2kL}$  with  $k$  denoting a bound-state momentum,  $L$  the IR length of the oscillator basis, and an integer  $n$ . We successfully tested the extrapolation formulas (and higher-order corrections) in simple potential models and for a realistic deuteron computed with interactions from chiral EFT. It would be interesting to probe and use these formulas in *ab initio* computations

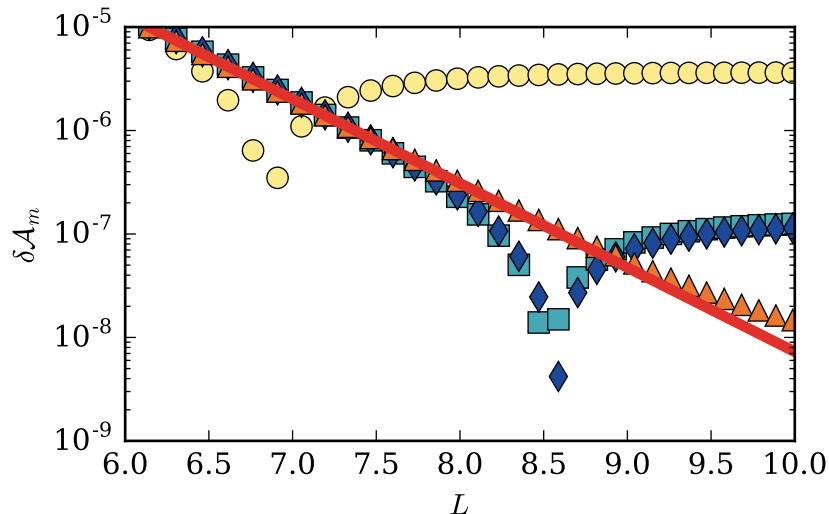


FIG. 6. (color online) The residual transition amplitude from fitting to increasing powers of  $(1/k_2L)$  in Eq. (35). The yellow dots represent a leading order fit ( $m = 0$ ), the light blue squares include also the  $(1/k_2L)$  term ( $m = -1$ ), the dark blue diamonds include also the  $(1/k_2L)^2$  term ( $m = -2$ ), and the orange triangles include also the  $(1/k_2L)^3$  term ( $m = -3$ ). The red, solid line represents  $e^{-2k_2L}$  where  $k_2$  is determined from a  $d$ -wave energy fit.

of finite nuclei. Our results for quadrupole transitions between bound states should also hold for transitions from bound states into narrow states close to the threshold. It would also be interesting to work out extrapolation formulas for transitions into arbitrary continuum states in the future.

### ACKNOWLEDGMENTS

We thank A. Ekström for providing us with matrix elements. This work was supported in parts by the U.S. Department of Energy, Office of Science, Office of Nuclear Physics under Grant No. DEFG02-96ER40963 (University of Tennessee) and Contract No. DE-AC05-00OR22725 (Oak Ridge National Laboratory), the National Science Foundation under Grant No. PHY-1516077, and by the US-Israel Binational Science Foundation under Grant No. 2012212.

- 
- [1] P. Navrátil, S. Quaglioni, I. Stetcu, and B. R. Barrett, “Recent developments in no-core shell-model calculations,” *Journal of Physics G: Nuclear and Particle Physics* **36**, 083101 (2009).
  - [2] B. R. Barrett, P. Navrátil, and J. P. Vary, “Ab initio no core shell model,” *Progress in Particle and Nuclear Physics* **69**, 131 – 181 (2013).
  - [3] M. Lüscher, “Volume Dependence of the Energy Spectrum in Massive Quantum Field Theories. 1. Stable Particle States,” *Commun. Math. Phys.* **104**, 177 (1986).
  - [4] R. J. Furnstahl, G. Hagen, and T. Papenbrock, “Corrections to nuclear energies and radii in finite oscillator spaces,” *Phys. Rev. C* **86**, 031301 (2012).
  - [5] I. Stetcu, B.R. Barrett, and U. van Kolck, “No-core shell model in an effective-field-theory framework,” *Physics Letters B* **653**, 358 – 362 (2007).
  - [6] G. Hagen, T. Papenbrock, D. J. Dean, and M. Hjorth-Jensen, “Ab initio coupled-cluster approach to nuclear structure with modern nucleon-nucleon interactions,” *Phys. Rev. C* **82**, 034330 (2010).
  - [7] E. D. Jurgenson, P. Navrátil, and R. J. Furnstahl, “Evolving nuclear many-body forces with the similarity renormalization group,” *Phys. Rev. C* **83**, 034301 (2011).
  - [8] S. N. More, A. Ekström, R. J. Furnstahl, G. Hagen, and T. Papenbrock, “Universal properties of infrared oscillator basis extrapolations,” *Phys. Rev. C* **87**, 044326 (2013).
  - [9] R. J. Furnstahl, G. Hagen, T. Papenbrock, and K. A. Wendt, “Infrared extrapolations for atomic nuclei,” *Journal of Physics G: Nuclear and Particle Physics* **42**, 034032 (2015).

- [10] K. A. Wendt, C. Forssén, T. Papenbrock, and D. Sääf, “Infrared length scale and extrapolations for the no-core shell model,” [Phys. Rev. C \*\*91\*\*, 061301 \(2015\)](#).
- [11] S. A. Coon, M. I. Avetian, M. K. G. Kruse, U. van Kolck, P. Maris, and J. P. Vary, “Convergence properties of *ab initio* calculations of light nuclei in a harmonic oscillator basis,” [Phys. Rev. C \*\*86\*\*, 054002 \(2012\)](#).
- [12] R. J. Furnstahl, S. N. More, and T. Papenbrock, “Systematic expansion for infrared oscillator basis extrapolations,” [Phys. Rev. C \*\*89\*\*, 044301 \(2014\)](#).
- [13] C. Cockrell, J. P. Vary, and P. Maris, “Lithium isotopes within the *ab initio* no-core full configuration approach,” [Phys. Rev. C \*\*86\*\*, 034325 \(2012\)](#).
- [14] C. Forssén, R. Roth, and P. Navrátil, “Systematics of  $2^+$  states in C isotopes from the no-core shell model,” [Journal of Physics G: Nuclear and Particle Physics \*\*40\*\*, 055105 \(2013\)](#).
- [15] P. Maris, J. P. Vary, and P. Navrátil, “Structure of  $A = 7-8$  nuclei with two- plus three-nucleon interactions from chiral effective field theory,” [Phys. Rev. C \*\*87\*\*, 014327 \(2013\)](#).
- [16] D. A. Varshalovich, A. N. Moskalev, and V. K. Khersonsky, [Quantum Theory of Angular Momentum](#) (World Scientific, Singapore, 1988).
- [17] D. Djajaputra and B. R. Cooper, “Hydrogen atom in a spherical well: linear approximation,” [European Journal of Physics \*\*21\*\*, 261 \(2000\)](#).
- [18] R. Machleidt and D.R. Entem, “Chiral effective field theory and nuclear forces,” [Physics Reports \*\*503\*\*, 1 – 75 \(2011\)](#).